



**HAL**  
open science

# Experimental observation and pressure drop modeling of plug formation in horizontal millifluidic hydraulic conveying

Marc Fischer, Étienne Gagnepain, Guillaume Dumazer

## ► To cite this version:

Marc Fischer, Étienne Gagnepain, Guillaume Dumazer. Experimental observation and pressure drop modeling of plug formation in horizontal millifluidic hydraulic conveying. *Physical Therapy Reviews*, 2024, 109 (4), pp.044906. 10.1103/PhysRevE.109.044906 . emse-04565964

**HAL Id: emse-04565964**

**<https://hal-emse.ccsd.cnrs.fr/emse-04565964v1>**

Submitted on 13 May 2024

**HAL** is a multi-disciplinary open access archive for the deposit and dissemination of scientific research documents, whether they are published or not. The documents may come from teaching and research institutions in France or abroad, or from public or private research centers.

L'archive ouverte pluridisciplinaire **HAL**, est destinée au dépôt et à la diffusion de documents scientifiques de niveau recherche, publiés ou non, émanant des établissements d'enseignement et de recherche français ou étrangers, des laboratoires publics ou privés.

# Experimental observation and pressure drop modelling of plug formation in horizontal millifluidic hydraulic conveying

Marc Fischer, Etienne Gagnepain, and Guillaume Dumazer

Mines Saint-Etienne, Univ Lyon, CNRS, UMR 5307 LGF, Centre SPIN, F - 42023 Saint-Etienne France

(Dated:)

The hydraulic conveying of glass beads was studied in a horizontal tube. At low flow rates, plugs could be observed moving across the tube whereas pseudo-plugs could be seen at higher flow rates. A statistical analysis of the plugs' and pseudo-plugs' velocities, and plugs' lengths observed was conducted. A transition of the propagation speeds distribution is established when the crossing over from plug to pseudo-plug regime is reached, where the peaked plug velocity distribution turns into a uniform pseudo-plug velocity distribution. On the other hand, the statistical distribution of plug lengths exhibits a log-normal mathematical shape.

The interpretation of the measured pressure drop evolution with the imposed flow rate by means of an effective viscosity shows an apparent shear-thinning effect coming from the dilution of the granular material. This approach provides a predictive tool for pressure drop calculation in the pseudo-plugs regime.

## I. INTRODUCTION

In contrast to pneumatic conveying widely used in industry to handle particulate material where solid particles are carried by an air stream, hydraulic conveying relies on the use of liquids such as water to transport solid matter over a given distance. Hydraulic conveying still plays an important role in our industrial world owing to its relatively low cost and lack of significant energy consumption with regards to the large distances it can potentially handle [1]. It is, for example, used to transport coal slurry [2], iron ore [3], phosphates [4], coal combustion products [5], and mineral wastes [6]. Moreover, the study of hydraulic conveying is intimately related to investigations into the transport of sediments in rivers [7, 8] and of sediments and sludge within sewers [9, 10]. While numerous empirical and semi-empirical formula have been developed for several decades alongside mechanical models [11–13], our understanding of hydraulic conveying remains imperfect, especially when it comes to the optimisation of industrial conveying solution [14, 15].

According to [1], horizontal hydraulic conveying is characterised by several regimes such as stationary bed, or moving-bed flow, heterogeneous suspension flow (with a vertical concentration gradient), and finally a pseudo-homogeneous suspension flow while the conveying speed grows larger at a constant solid concentration. Between the stationary-bed and moving-bed flow, we can observe travelling fluctuations of the bed height. In [16] a phenomenological description of various dense regimes is proposed for pneumatic conveying, as granular material and pneumatic gas velocity is varied. Several *plug flow* regimes are distinguished when the bed height fills locally the entire tube's cross section, forming *plugs* clearly separated from each other. *Slug flow* regime is mentioned when the granular matter is transported alongside long gas slugs [17] with large fluctuation in the particle concentration. Some authors [1, 18] also mention a *dune* flow

regime establishing from a dilute conditions as the fluid velocity is decreased. Granular heaps have been seen to form and travel at the surface of the granular bed driven by a saltation phenomenon. In geosciences dunes have been studied in details and a solid physical framework explaining dunes' displacement speed as well as dunes' wavelength can be found in the literature [19, 20]. Physical phenomena responsible for the displacement of granular particles at the surface of the bed due to viscous drag by the flowing fluid above is identical when it comes to describe the transport of sand particles by the wind, or industrial particulate material in a pneumatic conveying line. However, the geometrical confinement existing in a hydraulic or pneumatic conveying pipe starts to make a major difference when solid particles accumulate so that the tube's or pipe's cross-section is filled. For this reason the knowledge successfully developed for understanding dunes' formation and displacement at the surface of the Earth doesn't apply for dense regimes developing in pneumatic or hydraulic conveying.

Horizontal hydraulic and pneumatic conveying have a lot in common so that insights into one of the processes can often be profitably used for investigations of the other process [15, 21, 22].

A large variety of pneumatic conveying regimes exists [17] and the fluid superficial velocity and transported mass rate represent controlling parameters. In both hydraulic and pneumatic conveying the relationship between pressure drop and superficial gas velocity is established empirically for a series of mass rate values for a given particulate material and a conveying line [21]. For small superficial gas velocities the solid friction between solid particles and conveying line walls is the dominant dissipative phenomena and solid particles agglomerate. In these so called dense flow regimes solid particles agglomerate into granular waves also called plugs. It has been shown thanks to tracers that particle speed is smaller than the granular wave speed [23]. A pick-up mechanism is taking place where solid particles are collected at the front side of the propagating plug,

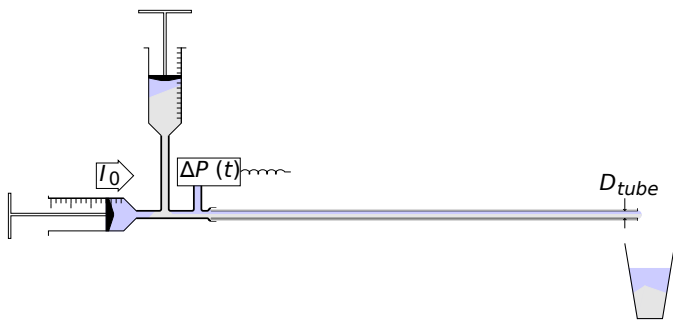


FIG. 1: Sketch of the experimental setup. An horizontal glass tube of inner diameter  $D_{tube}$  contains a mixture of water and grains. A syringe pump imposes a constant flow rate of water  $I_0$  whereas a second syringe filled with glass beads introduces the granular material into the stream at the tube's inlet where a pressure sensor is returning the measurement  $\Delta P(t)$ .

are transported over a given distance, before being deposited at the rear side of the plug and left behind [24, 25]. Although less investigated, studies have shown that hydraulic conveying rely on saltation mechanism as observed experimentally [26] as well as on a pick-up mechanism too [27, 28]. Similarly to what has been extensively studied in pneumatic conveying systems, hydraulic conveying crosses over from dense to dilute flow regimes [29] and pressure drop prediction has been approached numerically [15, 29].

On the other hand, for particle-laden flows, rheological studies of suspension have provided powerful descriptions of the complex relationship between shear stress with shear rate and solid particle concentration [30, 31]. A broad range of dry granular flow or granular suspension can find a useful interpretation thanks to recent rheological approaches in geosciences [32] or to treat industrial issues [33].

In the present study, we set out to investigate the horizontal hydraulic conveying of small glass beads at relatively small flow rates in order to improve our knowledge and comprehension of hydraulic conveying dense regimes in a millifluidic setting. In Section II, we present our experimental methodology. We show the results of our analysis of the appearance, behaviour and features of plugs and pseudo-plugs in Section III. In Section IV, we describe our treatment and analysis of the pressure drop profiles. We end this article with a conclusion and an outlook in Section V.

## II. EXPERIMENTAL SETUP

The experimental setup can be seen in Figure 1. The hydraulic transport of a granular phase is obtained experimentally by means of a syringe pump (Harvard ap-

paratus) imposing a fixed flow rate  $I_0$  of filtered water in a millifluidic tube of 590 mm length. A second syringe filled with glass beads of diameter  $d_{grain} \in [70 - 110] \mu\text{m}$  is used as a granular reservoir connected to the tube's inlet. The granular matter is falling by gravity into the stream of water coming from the syringe pump. A differential pressure sensor (Keller PD-23/8666.1) measures the pressure drop  $\Delta P$  between the tube's inlet and the atmosphere. The flow inside the tube is recorded by a camera with a 30 fps frequency. The experiments begin by setting up a steady flow containing only water. The granular matter is then poured at a constant rate into the stream of water ahead of the tube's inlet by opening a valve. The tube is initially empty of grains and the natural filling process leading to the formation of a uniform layer of sedimented grains requires a long time before completion. In order to accelerate the relaxation towards a steady hydraulic transport of grains, a quick granular flow is applied by pressing the syringe storing the granular matter. Once a rapid flow of suspended grains is obtained along the entire length of the tube the pressure on the syringe storing the grains is released and the suspension flow slows down. The suspended granular phase sediments then homogeneously in the tube. This experimental manipulation accounts for the pressure peak visible between the first plateau (corresponding to the Hagen-Poiseuille flow of pure water) and the second plateau (corresponding to the hydraulic transport of granular matter), as can be viewed in Figure 2.

The experiment ends when the water syringe pump is empty. The following flow rate values have been used: 1, 2, 3, 4, 5, 10, 15, and 20  $\text{mL}\cdot\text{min}^{-1}$ . The reproducibility of the observations has been assessed by performing each experiment three times. The present setup imposes a fixed mass rate of grains, since the vertical syringe storing the granular matter can either be closed or fully opened.

The experiments were then systematically recorded with a camera. The image treatment procedure is illustrated in Figure 3. First of all, the images are cropped and desaturated. A light intensity threshold is then employed to obtain a black and white picture, whereby the white areas indicate the presence of the white glass beads. For each abscissa  $x$  along the horizontal axis and at each time  $t$ , the height of granular matter (i.e. the number of white pixels) is calculated. This number is then converted into a black-and-white light intensity. The local amount of grains at a position  $x$  is thus converted into a grey scale where light values correspond to large heights of grains, whereas dark values correspond to small heights of grains and eventually, for black values, to the absence of grains. The temporal dynamics is then represented by means of a spatio-temporal diagram as shown in Figure 4. All granular profiles along the tube obtained after image treatment are stacked on top of each other from the top to the bottom as a function of time. Accordingly, the ordinate corresponds to the temporal axis developing downwards whereas the abscissae corresponds to the longitudinal coordinates.

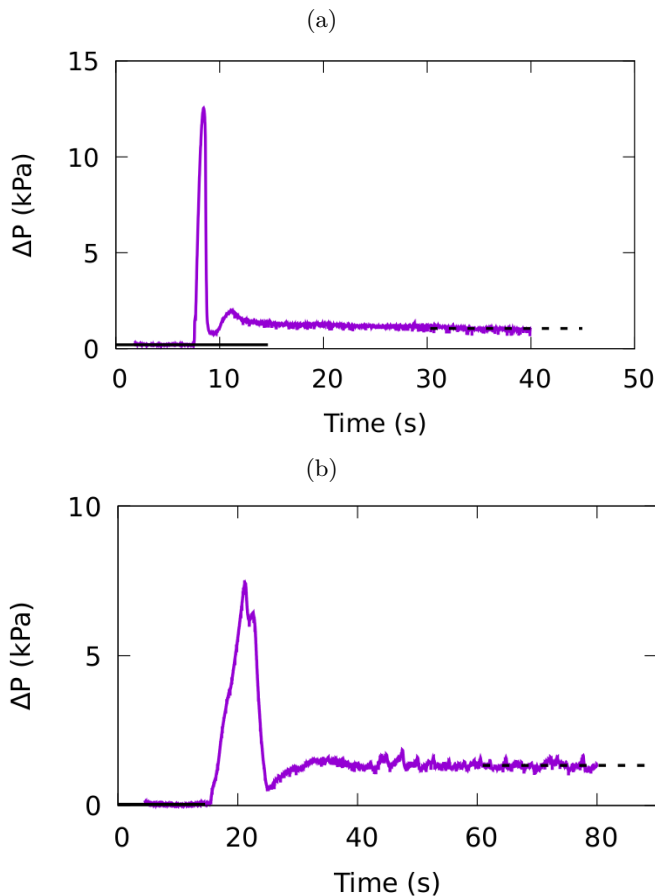


FIG. 2: Pressure time series measured with an imposed flow rate (a)  $I_0 = 10 \text{ mL}\cdot\text{min}^{-1}$  and (b)  $I_0 = 2 \text{ mL}\cdot\text{min}^{-1}$ . The solid and dashed lines mark the steady-state pressure plateaus obtained without any grains and with grains, respectively.

At the temperatures in our laboratory (which fluctuates between  $21^\circ \text{C}$  and  $24^\circ \text{C}$ ), we can take the following values for the density and dynamic viscosity of water:  $\rho_w = 997.62 \text{ kg/m}^3$  and  $\mu_w = 9.33 \cdot 10^{-4} \text{ Pa}\cdot\text{s}$ .

### III. PLUG ANALYSIS

#### A. Plug and pseudo-plug flow regimes

In these experiments we could observe the formation and propagation of *plugs* for flow rate values  $I_0 \leq 3 \text{ mL}\cdot\text{min}^{-1}$ . These *plugs* correspond to accumulated granular matter filling the tube from bottom to top over a certain length and moving in the flow direction, see the inclined white stripes in the spatio-temporal diagram in Fig. 4.

At larger flow rates  $I_0 \geq 3 \text{ mL}\cdot\text{min}^{-1}$  the sedimented bed appears to be dragged along the tube with no clear plug formed. However the spatio-temporal analysis shows that granular fronts with small amplitude are

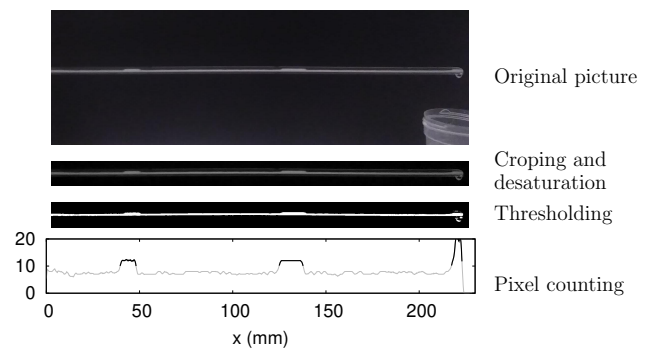


FIG. 3: Image treatment procedure applied to the original picture for  $I_0 = 1 \text{ mL}\cdot\text{min}^{-1}$ .

travelling. These displacements are evidenced by inclined lines in the spatio-temporal diagrams obtained for  $I_0 \geq 4 \text{ mL}\cdot\text{min}^{-1}$ , and only partially visible in the ones obtained for  $I_0 \in [2-3] \text{ mL}\cdot\text{min}^{-1}$ . These lines indicate that some fluctuations of the granular layer's height are propagating from left to right. These propagating fluctuations of the granular matter height will be denoted *pseudo-plugs* in the rest of the text.

A first quantity that can be measured from the spatio-temporal diagram is then the plugs' or pseudo-plugs' propagation speed  $v_{front}$  obtained from the slopes of their stripes, see Fig. 5. We also looked at the plugs' length  $\lambda$ . Note that in the case of pseudo-plugs with no clearly defined extensional size, a single velocity  $v_{front}$  is measured and no length can be defined in this case.

#### B. Statistical methodology

As can be seen in Figures 3 and 4, for flow rates smaller than  $3 \text{ mL}\cdot\text{min}^{-1}$ , plugs can be observed moving through the tube. However, for  $I_0 \geq 3 \text{ mL}\cdot\text{min}^{-1}$ , it becomes harder and harder to identify plugs, concurrently pseudo-plugs events become more frequent.

As a preliminary verification we performed a Mann-Whitney U test in order to ensure the similarities of the statistical properties of random variables such as the plugs' or pseudo-plugs' velocities  $v_{front}$  and plugs' lengths  $\lambda$  obtained for two different experiments with the same flow rate value. For every plug moving throughout the tube, we computed the three quartiles of the plug's length:  $q_{25}(\lambda)$ ,  $med(\lambda)$  and  $q_{75}(\lambda)$ , which are themselves random variables as they can vary from plug to plug. In order to test the similarity of the distribution of a random variable  $Y$  during two trials conducted under the same conditions, the Mann-Whitney U test considers the null hypothesis  $H_0: p(Y_1 < Y_2) = p(Y_1 > Y_2)$  against the hypothesis  $H_1$  that  $p(Y_1 < Y_2) \neq p(Y_1 > Y_2)$  at least for some values [34]. The results of the Mann-Whitney U test are shown in Table I. The experiments were conducted at an imposed flow rate  $I_0 = 1 \text{ mL}\cdot\text{min}^{-1}$  (trials

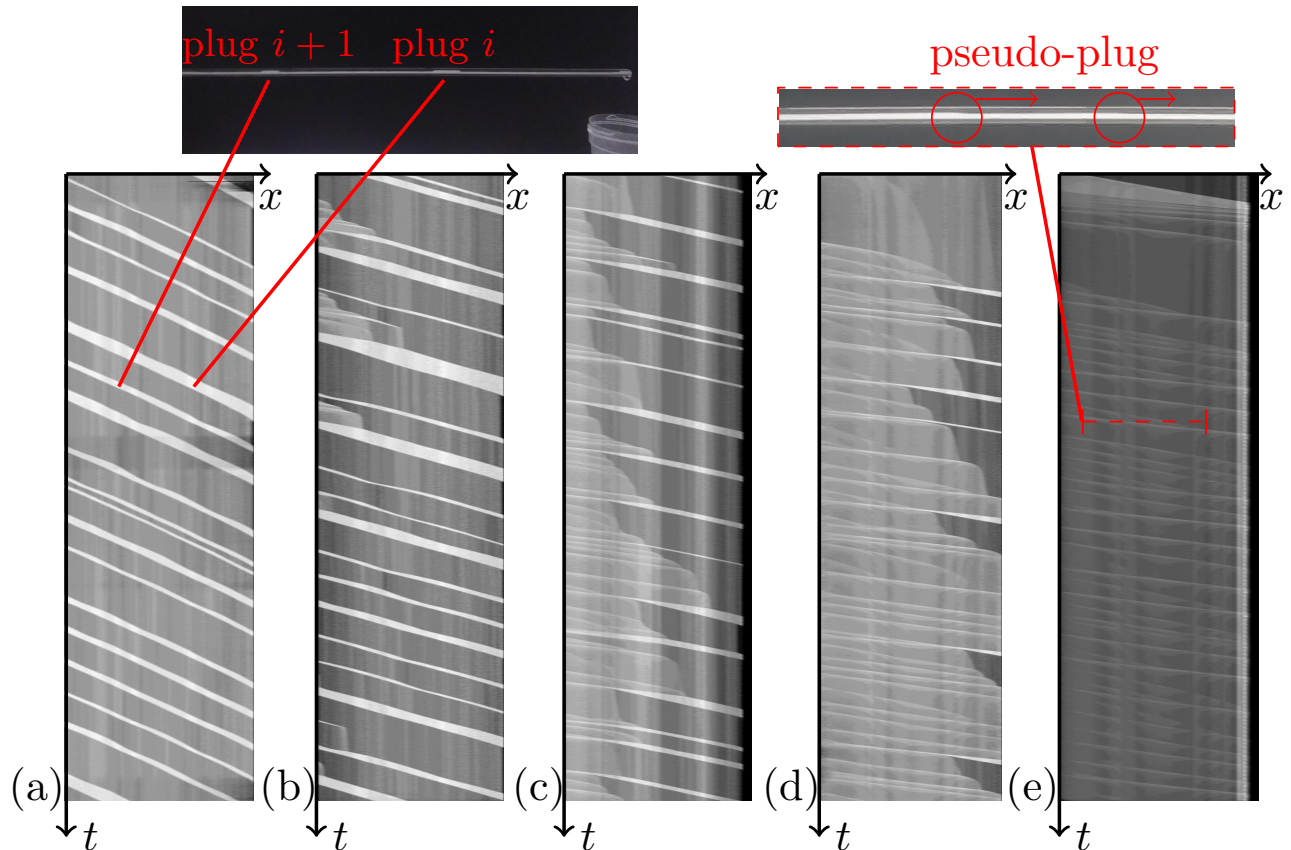


FIG. 4: Spatio-temporal diagrams obtained from a section of the tube of length 234 mm located left from the tube outlet for the following flow rate values (a)  $I_0 = 1 \text{ mL}\cdot\text{min}^{-1}$ , (b)  $I_0 = 2 \text{ mL}\cdot\text{min}^{-1}$ , (c)  $I_0 = 3 \text{ mL}\cdot\text{min}^{-1}$ , (d)  $I_0 = 4 \text{ mL}\cdot\text{min}^{-1}$ , and (e)  $I_0 = 5 \text{ mL}\cdot\text{min}^{-1}$ . Time goes downwards for 231 s.

Trials	$med(\lambda)$	$q25(\lambda)$	$q75(\lambda)$
1 - 1 $\text{mL}\cdot\text{min}^{-1}$ (trial1 - trial2)	3.90E-01	3.80E-01	3.50E-01
1 - 2 $\text{mL}\cdot\text{min}^{-1}$ (trial1 - trial3)	9.51E-04	1.85E-03	2.95E-04
1 - 2 $\text{mL}\cdot\text{min}^{-1}$ (trial1 - trial4)	3.65E-03	5.29E-03	3.02E-03
1 - 2 $\text{mL}\cdot\text{min}^{-1}$ (trial2 - trial3)	4.03E-05	1.06E-04	2.10E-05
1 - 2 $\text{mL}\cdot\text{min}^{-1}$ (trial2 - trial4)	8.29E-04	1.07E-03	5.37E-04
2 - 2 $\text{mL}\cdot\text{min}^{-1}$ (trial3 - trial4)	2.79E-01	2.31E-01	1.91E-01

TABLE I: Mann-Whitney U tests for the plugs' lengths  $\lambda$  done for series of observations performed at a flow rate  $I_0 = 1 \text{ mL}\cdot\text{min}^{-1}$  and  $I_0 = 2 \text{ mL}\cdot\text{min}^{-1}$ .

1 and 2) and for two series of observations at an imposed flow rate  $I_0 = 2 \text{ mL}\cdot\text{min}^{-1}$  (trials 3 and 4). If the value of the test becomes lower than a risk threshold set to  $\alpha = 0.05$  we have a quantitative sign that the two sets of observations may come from different statistical distributions as the probability of obtaining the results we see if the probability distributions are the same (hypothesis  $H_0$ ) is smaller than  $\alpha$ . The highest test values are obtained here for observations made with similar flow rate conditions, i.e. for trial 1 and 2 on the one hand, and for

trials 3 and 4 on the other hand. This confirms that we can safely analyse together the results of two observations obtained at the same flow rate.

The cumulative probability distribution function (cdf) of a random variable  $X$  is defined as  $F(x) = p(X \leq x)$ ; i.e. the probability that  $X$  takes on a value that is equal to or smaller than  $x$ . If we know  $n$  realisations of the random variable  $X$ , the empirical cumulative probability distribution function (ecdf) is defined as

$$F_n(x) = \frac{\text{Number of observations in the sample } \leq x}{n} = \frac{1}{n} \sum_{i=1}^n \mathbf{1}_{\{x_i \leq x\}}. \quad (1)$$

$F_n(x)$  converges towards  $F(x)$  when  $n$  tends to infinity.

### C. Results of the statistical analysis

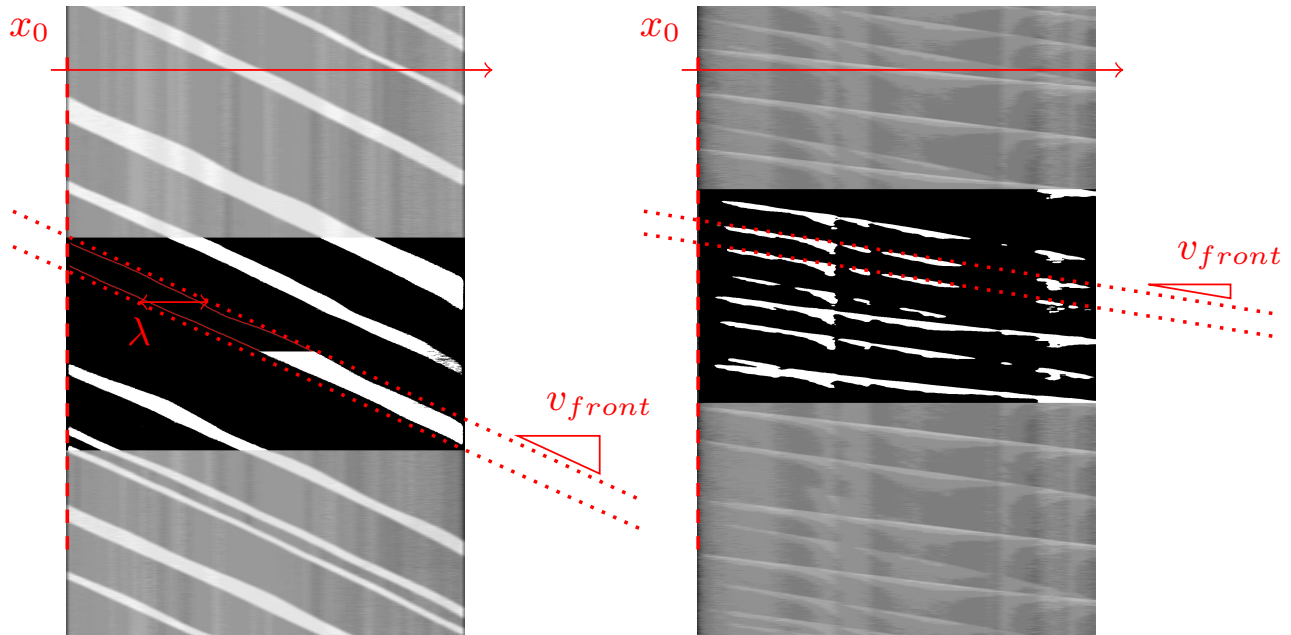


FIG. 5: Details of the spatio-temporal diagram obtained for a flow rate  $I_0 = 1 \text{ mL}\cdot\text{min}^{-1}$  during 85 s (left) and  $I_0 = 5 \text{ mL}\cdot\text{min}^{-1}$  during 79 s (right). Thin solid red lines show the boundaries of the central white stripe after thresholding and contour detection for plugs travelling (left). The two upper and lower slopes in dashed lines indicate respectively the front- and the rear-velocities of the travelling plug. Only the front velocity  $v_{front}$  will be considered in this work. Plug's length  $\lambda$  is obtained as the distance between the two front- and rear-velocity slopes. For pseudo-plugs propagation (right) only velocities  $v_{front}$  can be defined.

*a. Plugs' and pseudo-plugs' velocities.* The velocities are measured from spatio-temporal diagrams. It corresponds to a random variable because it will vary from plug to plug in an unpredictable fashion.  $med(v_{front})$  is then the median values of  $v_{front}$  when all the plugs observed at the same flow rate are considered. Empirical cumulative functions for the plugs' and pseudo-plugs' velocities present a clear difference, see Fig. 6(a). Plugs are progressing with very narrow velocity distributions, exhibiting little variations as shown by the steep step in the cumulative functions (solid lines in Fig. 6(a)). Pseudo-plugs are presenting conversely some variations of their velocities from pseudo-plug to pseudo-plug. The almost linear behaviour of the cumulative functions for pseudo-plugs' velocities points to a uniform pseudo-plugs' velocities distribution between two extreme values approximately equal to  $\frac{1}{2}med(v_{front})$  and  $\frac{3}{2}med(v_{front})$ . Both plugs and pseudo-plugs propagation dynamics appear to be determined by a single parameter being the median propagation velocity as shown by the collapse of cumulatives obtained for the plugs, i. e. for  $I_0 \in [1 - 3] \text{ mL}\cdot\text{min}^{-1}$  on the one hand, and for the pseudo plugs, i. e. for  $I_0 \in [3 - 5] \text{ mL}\cdot\text{min}^{-1}$  on the other hand. The evolution of  $med(v_{front})$  for various imposed flow rates is shown in Fig. 6(b). Plugs have a median velocity increasing with the imposed flow rate. The solid line in

Fig. 6(b) is a guide for the eye showing how the average fluid velocity increases linearly with the flow rate if half of the tube cross section is obstructed by sedimented grains. This average velocity seems to be a fairly good estimate for plugs' velocities. Pseudo-plugs exhibit a counter intuitive behaviour with a propagation velocity decreasing with the imposed flow rate. However their values stay within some limits given by average fluid velocity in a fully open and 25% open cross section. This decreasing behaviour could correspond to a decreasing obstruction of the tube's cross section due to the sedimented bed erosion increasing with the imposed flow rate. The increasing tube's cross sectional aperture leads to a decreasing fluid velocity displacing pseudo-plugs.

*b. Plugs' lengths.* As for plugs' and pseudo-plugs' velocity, plugs' length  $\lambda$  are measured from spatio-temporal diagrams and corresponds to a random variable as they vary from plug to plug. Its median value is noted  $med(\lambda)$ . Figure 7(a) shows the empirical cumulative function of the plugs' lengths  $\lambda$  for  $I_0 = 1, 2$  and  $3 \text{ mL}\cdot\text{min}^{-1}$ . The plugs' length dimensionless variable  $\lambda^* = (\lambda/med(\lambda))^{1/\sigma}$  is obtained from the median value of the plugs' lengths  $med(\lambda)$  and from the log-normal distribution parameter  $\sigma = \sqrt{2(\ln(\langle\lambda\rangle) - \ln(med(\lambda)))}$ , the plugs' length mean value being  $\langle\lambda\rangle$ . An increase of the median plugs' length  $med(\lambda)$  and of the standard devia-

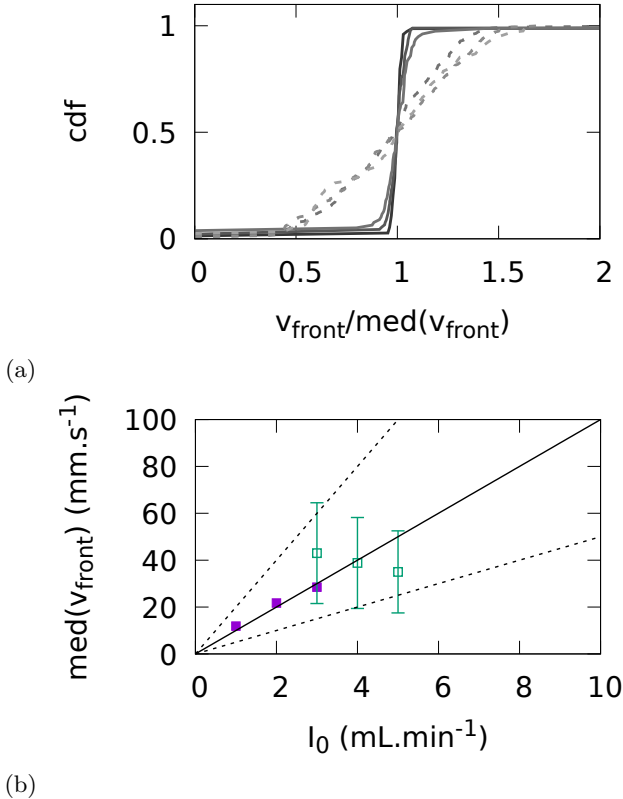


FIG. 6: (a) Empirical cumulative functions for plugs' (solid lines) and pseudo-plugs' (dashed lines) velocities normalized by the median velocities of each distributions. The shade of grey indicates the imposed flow rate ranging from  $1 \text{ mL}\cdot\text{min}^{-1}$  (dark grey) to  $5 \text{ mL}\cdot\text{min}^{-1}$  (light grey). (b) Median velocity values of plugs (solid symbols) and pseudo-plugs (open symbols) obtained for different imposed flow rate values. Error bars associated with pseudo-plugs median velocities correspond to the observed minimal and maximal velocity values. The lines are guide for the eye giving the expected fluid velocity averaged over the cross sectional full aperture (bottom dashed line), 50% aperture (solid line) and 25% aperture (top dashed line).

tion of the distribution can be observed with the imposed flow rate  $I_0$ , see Fig. 7 (b).

The observed plugs' length distributions for  $I_0 \in [1 - 3] \text{ mL}\cdot\text{min}^{-1}$  fluctuate around the normalized log-normal distribution. The asymptotic distribution of a random splitting process corresponds to a log-normal shape [35, 36]. This observation could lead to further modelling assumption about the plugs' formation mechanism.

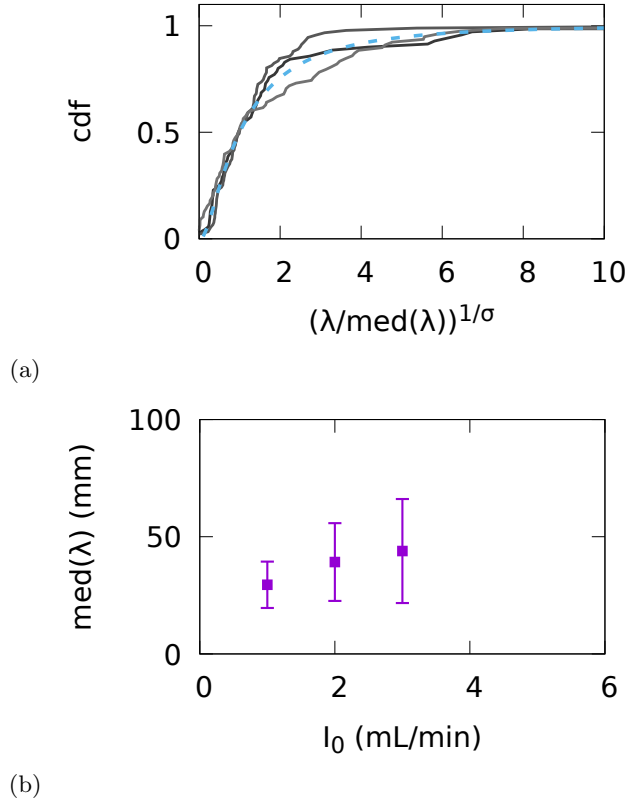


FIG. 7: (a) Normalized empirical cumulative functions of the plugs' length  $(\lambda/\text{med}(L))^{1/\sigma}$  (solid lines), and normalized cumulative function for a log normal distribution (dashed line). The shades of gray gives the flow rate values ranging from  $1 \text{ mL}\cdot\text{min}^{-1}$  (dark grey) to  $3 \text{ mL}\cdot\text{min}^{-1}$  (lighter gray). (b) Median and variance values used for normalization, resp. solid symbols and error bars.

## IV. PRESSURE DROP ANALYSIS

### A. Evolution of the pressure drop

Pressure measurements time-series during one experiment show two plateaus separated by a sudden pressure drop peak corresponding to the experimental manipulation leading to the uniform introduction of the granular material into the tube, see Fig. 2. First plateau corresponds to the pressure drop due to the pure water flow along the tube at a given flow rate  $I_0$ . The final plateau corresponds to the pressure drop resulting from the hydraulic conveying of granular matter. One can observe the increase in pressure drop from pure water flow to hydraulic conveying.

As can be seen on Figure 8 the pressure drop measurements for pure water (disks) follow the Hagen-Poiseuille

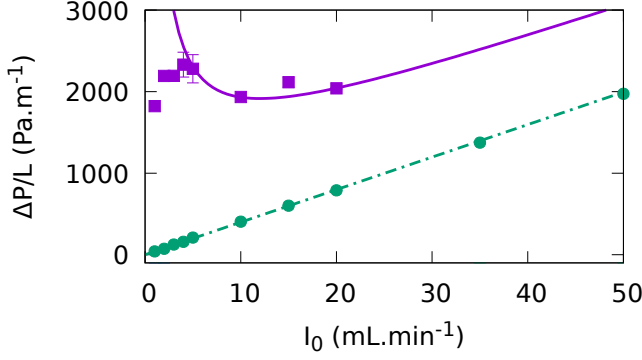


FIG. 8: Pressure drop measurements for pure water (disks) and for hydraulic conveying of glass beads (squares) as function of the imposed flow rate  $I_0$ . Each experiment were executed two to three times and the error bars show the minimum and maximum measurements. The solid line gives the expected pressure drop for a suspension with the Maron-Pierce correlation and a flow-rate dependent solid filling fraction. The dash-dotted line gives the expected pressure drop obtained with the Hagen-Poiseuille formula for pure water.

formula (dash-dotted line) :

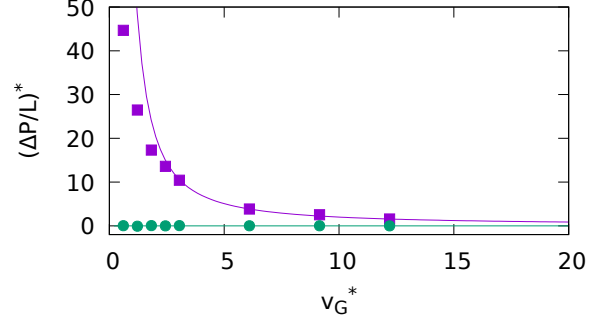
$$(\Delta P/L)_{HP} = \frac{128\mu_w I_0}{\pi D_{tube}^4}. \quad (2)$$

Experiments have been executed two to three times to test the reproducibility of the measurements. For each imposed flow rate values, error bars show maximum and minimum values and squares are located at the mean values. After granular matter is introduced in the flow, an increase in the pressure drop has been observed for every imposed flow rate values. The relative difference between the pressure drop for pure water and for granular matter conveying is however decreasing.

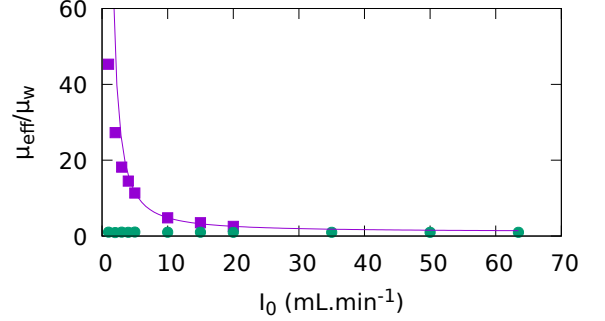
In this system a competition exists between the gravitational force leading to the sedimentation of the granular matter on the bottom side of the tube on the one hand, and the viscous drag leading to the conveying of the granular matter along the tube on the other hand. So we propose to build a dimensionless velocity from the ratio between the mean pure fluid velocity in the tube in the absence of grains,  $v_G = 4I_0/(\pi D_{tube}^2)$ , and the sedimentation velocity of a single grain in the fluid,  $v_{sed} = \Delta\rho g d_{grains}^2/(18\mu_w)$ :

$$v_G^* = \frac{72I_0\mu_w}{\pi D_{tube}^2 \Delta\rho g d_{grains}^2}. \quad (3)$$

We also suggest here to consider the pressure drop measurements  $(\Delta P/L)_{meas}$  when granular matter is introduced as a perturbation to the nominal pressure drop



(a)



(b)

FIG. 9: (a) Reduced pressure drop  $(\Delta P/L)^*$  as function of the dimensionless velocity  $v_G^*$  for pure water (disks) and granular conveying (squares). The solid line gives the zero ordinate base line Hagen-Poiseuille prediction.

(b) Effective viscosity ratio, calculated from the pressure drop measurement  $\mu_{eff}$  with pure fluid (disks) and with granular conveying, to the nominal fluid viscosity  $\mu_w$  as function of the imposed flow rate  $I_0$ . The solid line gives the effective viscosity ratio given by the Maron-Pierce correlation with our flow rate dependent filling fraction model.

$(\Delta P/L)_{HP}$  for pure water given by the Hagen-Poiseuille formula in Eq.( 2). So we consider the reduced pressure drop :

$$\left(\frac{\Delta P}{L}\right)^* = \frac{(\Delta P/L)_{meas} - (\Delta P/L)_{HP}}{(\Delta P/L)_{HP}}$$

Figure 9 (a) shows the evolution of the reduced pressure drop which gives the relative increase with respect to the pressure drop for pure fluid. The measurements made with pure fluid agree with the prediction from the Hagen-Poiseuille formula in Eq. (2) whereas the measurements made in hydraulic conveying conditions asymptotically converge towards the Hagen-Poiseuille prediction for large velocities  $v_G^*$ . On the contrary the reduced pressure drop seems to diverge as  $v_G^*$  tends to zero.

The Figure 9(b) shows the evolution of the effective viscosity  $\mu_{eff}$  divided by the nominal water viscosity. The effective viscosity  $\mu_{eff}$  corresponds to the viscosity value required so that the Hagen-Poiseuille formula's prediction corresponds to the pressure drop measurements

:

$$\mu_{eff} = \left( \frac{\Delta P}{L} \right)_{meas} \frac{\pi D_{tube}^4}{128 I_0}. \quad (4)$$

The hydraulic conveying pressure drop asymptotic trend towards the Hagen-Poiseuille prediction could be explained by the decreasing filling fraction in solid materials obtained for large flow rates. Indeed the solid mass rate  $w$  is determined by the tubings and granular material reservoir syringe diameters which does not change with the flow rate  $I_0$ . A rapid modelling of the filling fraction  $\phi$  could be derived from these two parameters :

$$\phi = \frac{w/\rho_g}{w/\rho_g + I_0}, \quad (5)$$

with the solid volume rate  $w/\rho_g$  and the fluid volume rate  $I_0$ . The effective viscosity of a suspension is an increasing function of the filling fraction in solid material [30, 31]. In particular the Maron-Pierce correlation [30] gives a satisfying match to pressure drop experimental measurements and numerical modelling out of a relatively simple mathematical formula :

$$\mu_{eff}/\mu_w = (1 - \phi)^{-2}. \quad (6)$$

Putting together eqs. (5) and (6) an analytical formula can be derived to predict the observed pressure drop measurements in our system :

$$\left( \frac{\Delta P}{L} \right)_{MP} = \frac{128 I_0}{\pi D_{tube}^4} \mu_w \left( 1 - \frac{w/\rho_g}{w/\rho_g + I_0} \right)^{-2}. \quad (7)$$

This formula reproduces the observations for hydraulic conveying with a rather good accuracy, see the solid line in Fig. 9(b). For flow rate values  $I_0 \geq 3$  mL.min<sup>-1</sup>, the decreasing concentration in granular matter leading to a decreasing effective viscosity is well captured by the equation (7). For lower flow rate values  $I_0 \leq 3$  mL.min<sup>-1</sup> the prediction overestimates the measurements. Although Equation (7) provides here a very satisfying prediction for the pressure drop in nearly homogeneous horizontal hydraulic conveying from very dilute conditions at large flow rates down to semi-dense conditions with travelling pseudo-plugs, the heterogeneous travelling plug structure may be based on other physical phenomena.

A better estimation of the effective viscosity and pressure drop in plugs regime would require a better modelling of the various dissipative processes in heterogeneous hydraulic conveying, see [37]. The pressure drop increase with the imposed flow rate observed in plugs regime is consistent with the Ergun's equation derived for flow through packed columns [38]. The pressure drop increase indicates then that the fluid is flowing with a faster velocity than the plugs' speed.

## V. CONCLUSION AND OUTLOOK

While heterogeneous dense solid flows in hydraulic conveying systems present the advantage of causing less attrition and erosion than nearly homogeneous dilute flows, they are not as well understood as the latter in part due to the complex frictional interaction with the confining walls. The purpose of the present study was to improve our understanding of these dense flow regimes, and their transition towards dilute regimes. The hydraulic conveying of glass beads in a millifluidic tube was investigated through the systematic measurements of the pressure drop and the production of spatio-temporal diagrams from video recording. A full-fledged plug flow regime can be seen at a flow rate of  $I_0 \in [1-3]$  mL.min<sup>-1</sup> whereas flow rates  $I_0 \geq 3$  mL.min<sup>-1</sup> exhibit pseudo-plugs propagation regime.

For the lowest flow rate values here  $I_0 \leq 3$  mL.min<sup>-1</sup> the Archimede's number  $Ar = 14.7$  and the particle's Reynolds number  $Re \leq 1.6$  would correspond to a *plug-1* regime according to [16]. However the phenomenology observed here doesn't really match this particular regime as *plug-1* type is supposed to travel across and leave behind its passage an empty tube. In our observations the phenomenology of the observed plugs is closer to the *plug-2* type despite the small Archimede's number value. A difference between gas flow used in pneumatic conveying and the liquid flow used in the present hydraulic conveying study probably explains this inconsistency. For larger flow rates  $I_0 \geq 3$  mL.min<sup>-1</sup> the Reynolds number  $Re \geq 1.6$  for the same Archimede's number value, points towards a so-called *dune* regime in the literature. This regime has been studied in pneumatic [16] or in hydraulic conveying system [18] experimentally or numerically [1]. It would be of great interest to revisit these regimes, that has been denoted here *pseudo-plugs* as they seem to correspond to precursors of plugs, with the physical approach developed for studying geophysical dunes [19, 20]. Experimental observations with close-up images capture and analysis should help to clarify this.

Plugs' travelling velocities and length were statistically studied for various imposed water flow rate values. Plugs' and pseudo-plugs' velocity distributions centered around the median travelling velocity appeared to correspond respectively to a very steep distribution and to a uniform distribution with two extrema. The averaged flow velocity calculated with the half filled tube assumption seems to correspond to the median velocity determining the plugs' velocity distribution. In the case of pseudo-plugs, the median velocity which determines the width of the uniform distribution as well as its center, corresponds to the averaged flow velocity in the tube with a decreasing filling fraction as the increasing imposed flow rate is responsible for an increasing erosion of the sedimented bed.

The plugs' length distribution has been seen to follow a log-normal distribution which is typical for random splitting processes. Here the median value and its variance

increases as the flow rate increases. This statistical observation could help future modelling approaches to explain plugs' formation process.

Our experimental results expand numerical observations showing an increase in plugs' length and speed of the front plugs as the superficial velocity increases [39] with a statistical approach made possible with the large number of plugs studied. The effect of the flow rate on the pressure drop of the water-solid flow has also been studied. An asymptotic trend towards solid-free fluid flow has been recovered for large flow rate values due to the increasing dilution of the solid whose mass rate remains fixed whereas the fluid flow rate increases. In the pseudo-plugs regime, the fluidization of the granular matter allows to use filling fraction dependent effective viscosity models for granular suspension in order to obtain a good predictor of the pressure drop. The pressure drop measurements in the plug regime resist to a simple modelling which considers solid friction at the interface between plugs and tube's walls, and viscous dissipation between two plugs. A more detailed modelling taking into ac-

count tribological description at the interface between the travelling plug and the tube's wall together with a stress redirection within the granular material inside the plug and the viscous drag seems to be necessary here [37]. Further experimental observations with different hydraulic or pneumatic conveying systems would be of great interest to expend and give corrections to the present model. This work on hydraulic conveying of glass beads in a millifluidic tube has shown interesting analogies with pneumatic conveying of granular materials. In the future it would be of great interest to delve into the analogies and differences between the two systems as some unifying laws could be discovered [16, 21].

## VI. CONTRIBUTION

Etienne Gagnepain conducted and interpreted the experiments, Marc Fischer developed and applied the statistical methodology and Guillaume Dumazer supervised the whole project.

### References

- 
- [1] M. Zhou, S. Kuang, K. Luo, R. Zou, S. Wang, and A. Yu, *Powder Technology* **373**, 543 (2020).
  - [2] Z. Li-an, C. Ronghuan, and W. Tieli, in *IOP Conference Series: Earth and Environmental Science*, Vol. 113 (IOP Publishing, 2018) p. 012163.
  - [3] N. Kumar, M. K. Gopaliya, and D. Kaushal, *Particulate Science and Technology* **37**, 232 (2019).
  - [4] X. Li, L. Guo, and W. Xu, in *Journal of Physics: Conference Series*, Vol. 1626 (IOP Publishing, 2020) p. 012179.
  - [5] R. Rani and M. K. Jain, *Particulate Science and Technology* **37**, 123 (2019).
  - [6] L. Pullum, D. V. Boger, and F. Sofra, *Annual Review of Fluid Mechanics* **58**, 157 (2018).
  - [7] F. Osanloo, M. R. Kolahchi, S. McNamara, and H. J. Herrmann, *Physical Review E* **78**, 011301 (2008).
  - [8] M. Houssais, C. P. Ortiz, D. J. Durian, and D. J. Jerolmack, *Physical Review E* **94**, 062609 (2016).
  - [9] R. Ashley and M. Verbanck, *Journal of hydraulic research* **34**, 753 (1996).
  - [10] B. C. O'Kelly, in *Proceedings of the Institution of Civil Engineers-Municipal Engineer*, Vol. 157 (Thomas Telford Ltd, 2004) pp. 193–197.
  - [11] R. Durand, Intern. Assoc. Hydr. Res., 5th Congr. Minneapolis, 1953 (1953).
  - [12] D. Newitt, *Trans. Instn Chem. Engrs* (1955).
  - [13] K. C. Wilson, G. R. Addie, A. Sellgren, and R. Clift, *Slurry transport using centrifugal pumps* (Springer Science and Business Media, 2006).
  - [14] A. Uzi and A. Levy, *Powder Technology* **326**, 302 (2018).
  - [15] B. Ismael, *Fluid-und Feststofftransport in Rohrsystemen und Pumpstationen* (Dresden, 2021).
  - [16] H. Kalman and A. Rawat, *Chemical Engineering Science* **211**, 115256 (2020).
  - [17] E. Rabinovich and H. Kalman, *Powder Technology* **207**, 119 (2011).
  - [18] L. Borzone, *Chem. Eng. Comm.* **197**, 1215 (2010).
  - [19] F. Charru, B. Andreotti, and P. Claudin, *Annual Review of Fluid Mechanics* **45**, 469 (2013).
  - [20] M. Ouriemi, P. Aussillous, and E. Guazzelli, *J. Fluid Mech.* **636**, 321 (2009).
  - [21] H. Kalman, D. Portnikov, O. G. Gabrieli, and N. M. Tripathi, *Powder Technology* **354**, 485 (2019).
  - [22] M. do Carmo Ferreira, J. T. Freire, and G. Massarani, *Powder technology* **108**, 46 (2000).
  - [23] O. Orozovic, A. Lavrinec, Y. Alkassar, K. Williams, M. Jones, and G. Klinzing, *Powder Technology* **351**, 84 (2019).
  - [24] J. Li, C. Webb, S. Pandiella, G. M. Campbell, T. Dyakowski, A. Cowell, and D. McGlinchey, *Chemical Engineering and Processing: Process Intensification* **44**, 167 (2005).
  - [25] S. Shaul and H. Kalman, *Powder Technology* **272**, 322 (2015).
  - [26] P. Vlasák, Z. Chara, J. Krupicka, and J. Konfrst, *Journal of Hydrology and Hydromechanics* **62**, 241 (2014).
  - [27] L. Wang, A. Goharzadeh, and P. Rodgers, in *AIP Conference Proceedings*, Vol. 1376 (American Institute of Physics, 2011) pp. 351–353.
  - [28] Z. Chara, P. Vlasak, J. Konfrst, and B. Kysela, in *AIP Conference Proceedings*, Vol. 1648 (AIP Publishing LLC, 2015) p. 030021.
  - [29] E. Papista, D. Dimitrakakis, and S. Yiantsios, *Industrial and engineering chemistry research* **50**, 630 (2011).
  - [30] J. Stickel, Jonathan and L. Powell, Robert, *Annual Review of Fluid Mechanics* **37**, 129 (2005).
  - [31] E. Guazzelli and O. Pouliquen, *Journal of Fluid Mechanics* **852**, P1 (2018).
  - [32] J. Jerolmack, Douglas and E. Daniels, Karen, *Nature Reviews Physics* **1**, 716 (2019).
  - [33] C. Pierlot, H. Hu, C. Reeb, J. Bassetti, M. Bertin,

- D. Lambertin, C. Davy, and V. Nardello-Rataj, *Chemical Engineering Science* **255**, 117635 (2022).
- [34] H. B. Mann and D. R. Whitney, *The annals of mathematical statistics*, 50 (1947).
- [35] A. N. Kolmogorov, *Dokl. Akad. Nauk SSSR* **31**, 99 (1941).
- [36] A. F. Filippov, *Theory of Probability and its Applications* **6**, 275 (1961).
- [37] S. Shaul and H. Kalman, *Powder Technology* **256**, 310 (2014).
- [38] S. Ergun, *Chemical Engineering Progress* **48**, 89 (1952).
- [39] S. Kuang, K. Chu, A. Yu, Z. Zou, and Y. Feng, *Industrial and Engineering Chemistry Research* **47**, 470 (2008).